Perovskite Solar Cells Using Carbon Nanotubes Both as Cathode and as Anode

Il Jeon[1†], Seungju Seo[1†], Yuta Sato[2], Clement Delacou[1], Anton Anisimov[3], Kazu Suenaga[1,2], Esko I. Kauppinen[4], Shigeo Maruyama[1,5]*, Yutaka Matsuo[1,6]**

[1]Department of Mechanical Engineering, School of Engineering, The University of Tokyo, 7-3-1 Hongo, Bunkyo-ku, Tokyo 113-8565, Japan

[2] Nanomaterials Research Institute, National Institute of Advanced Industrial Science and Technology (AIST), Ibaraki 305-8565, Japan

[3] Canatu Ltd., Konalankuja 5, FI-00390 Helsinki, Finland

[4] Department of Applied Physics, Aalto University School of Science, FI-00076 Aalto, Finland

[5] Research Institute for Energy Conservation, National Institute of Advanced Industrial Science and Technology (AIST), Ibaraki 305-8564, Japan

[6]Hefei National Laboratory for Physical Sciences at Microscale, University of Science and Technology of China, 96 Jinzhai Road, Hefei, Anhui 230026, China

Correspondence to: esko.kauppinen@aalto.fi, +358 40-509-8064 (E.K), maruyama@t.u-photon.ac.jp, +81 3-5841-6421 (S.M.), matsuo@photon.t.u-tokyo.ac.jp, +81 3-5841-0978 (Y.M.)

ABSTRACT

Organic-inorganic halide perovskite solar cells have received much attention because they achieve high power conversion efficiency while providing the advantages of thin-film solar cells, namely, solution processability and potentially low fabrication cost. However, at the current level of halide perovskite solar cell technology, these advantages cannot be maximized due to structural and material limitations. Here, we provide a solution to these problems by replacing conventional metal and metal oxide electrodes with carbon nanotube electrodes. We also simplified the structure to achieve entirely solution-processable perovskite solar cells. Through this study, we demonstrated the function of carbon nanotubes as both the anode and cathode in perovskite solar cells. Economic modeling suggests that this novel architecture reduces costs dramatically. This work realizes innovations in the materials, costs, and processing of inverted-type perovskite solar cells.

INTRODUCTION

In recent years, organic-inorganic halide perovskite solar cells (PSCs)[1-4] have gained ground, reaching certified power conversion efficiencies (PCEs) of over 22%.[5,6] Such high performance is now leading many groups to consider commercialization of PSCs in light of their low-cost solution processability[7,8] and flexiblity.[9,10] Indeed, one of the most attractive aspects of solution-processed solar cells such as PSCs is the prospect of low-cost module processing via high-throughput printing with large-area coverage compared with wafer-based silicon solar cells.[11,12] While the problem of high-temperature processing can be avoided by adopting an inverted planar heterojunction architecture,[13] there are still several obstacles hindering the commercialization of

PSCs. First, scarce indium tin oxide (ITO) and costly metal electrodes are thermally deposited under vacuum, limiting scalability and the potential for minimizing costs.[14–16] In addition, the production of solution-processed photovoltaic devices to date has been done in non-continuous sheet-to-sheet (S2S) or roll-to-roll (R2R) processes,[17–21] which cause physical and electrostatic damage[22] and increase setup and running costs.[23–25]

A promising approach to overcoming the above limitations is to use all-carbon electrodes as well as entirely solution-based inner materials. Device performance is comparable between carbon electrodes and ITO or metal electrodes.[26–29] Also, it is possible to construct PSCs using entirely solution-processable layers, with only a minor loss of PCE.[10] The use of carbon electrodes and entirely solution-processed structures will lead to a dramatic reduction in processing costs via compatibility with continuous roll-to-product (R2P) processing instead of R2R or S2S processing.[16] In this work, we fabricated all-carbon nanotube (CNT) electrode-based PSCs that employ fully solution-processed layers (Figure 1). This study has two central aims: to demonstrate the use of CNT films as both the anode and cathode and to devise an entirely solution-processed configuration with a rational cost analysis for the fabrication process. We show that [6,6]-phenyl C_{61}-butyric acid methyl ester ($PC_{61}BM$)-soaked CNTs can function as the cathode via *n*-type doping, and also that poly(3-hexylthiophene-2,5-diyl) (P3HT)-soaked CNTs can function as the anode, playing a role in energy alignment. Our flexible fully solution-processed all-CNT-electrode PSCs, with a configuration of CNT-P3HT/poly(3,4-ethylenedioxythiophene):polystyrene sulfonate (PEDOT:PSS) /$CH_3NH_3PbI_3$ ($MAPbI_3$)/CNT-$PC_{61}BM$, gave a PCE of 7.32% and had good mechanical flexibility. The cost of materials in this configure was 33% of that of conventional devices, according to a cost analysis. The total

fabrication cost would be decreased even further if we were to also consider setup costs, maintenance costs, and processing time.

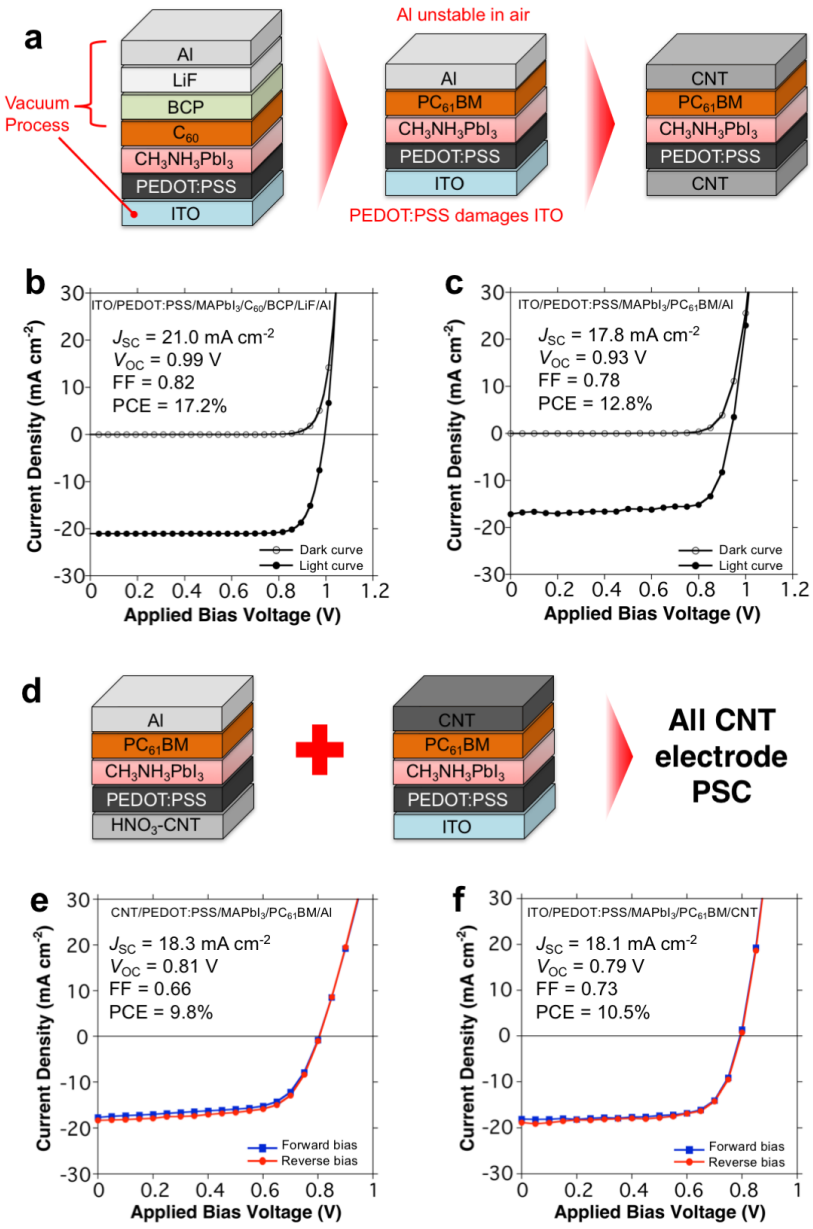

Figure 1. (**a**) Schematic illustrations of a conventional device, a conventional device without vacuum-deposited ETLs, and the proposed device. *J*–*V* curves of (**b**) the conventional device and (**c**) the conventional device without vacuum-deposited ETLs. (**d**) Schematic illustrations of a

device in which a HNO_3-doped CNT electrode was used as the anode instead of ITO and a device in which a CNT electrode was used as the cathode instead of metal. Forward (red) and reverse (blue) bias *J–V* curves of (**e**) the HNO_3-doped CNT anode-based device and (**f**) the CNT cathode-based device.

EXPERIMENTAL SECTION

Synthesis of CNT Films. Randomly oriented CNT networks with high purity and long nanotube bundle length can be synthesised by the aerosol chemical vapour deposition (CVD) method. The floating catalyst aerosol CVD was carried out in a scaled-up reaction tube with a diameter of 150 mm. The catalyst precursor was vaporised by passing ambient temperature CO through a cartridge filled with ferrocene powder. To obtain stable growth of CNTs, a controlled amount of CO_2 was added with the carbon source (CO). CNTs were directly collected downstream of the reactor by filtering the flow through a nitrocellulose or silver membrane filter (Millipore Corp., USA; HAWP, 0.45 μm pore diameter). The flow containing ferrocene vapour was then introduced into the high-temperature zone of a ceramic tube reactor through a water-cooled probe and mixed with additional CO. Ferrocene vapour was thermally decomposed in the gas phase of the aerosol CVD reactor at the 880 ˚C. The CO gas was supplied at 4 L min^{-1} and decomposed on the iron nanoparticles, resulting in growth of CNTs. The as-synthesised CNTs were collected by passing the flow through microporous filters at the downstream of the reactor, while the transparency and sheet resistance was controlled by varying the collection time. The collected CNT networks were transferred to a variety of substrates through the dry press-transfer process. The FC-CVD synthesised and dry deposited CNT networks were of high purity. Furthermore, as the process requires no sonication based dispersion steps the resulting CNT network consisted of exceptionally long CNTs.

Anode preparation. ITO substrates with size 15 × 15 mm^2 with a sheet resistance of 6 Ω/sq. (Techno Print Co., Ltd.) were sonicated in cleaning surfactant (Semi Clean, M-Lo), water, acetone and 2- isopropanol for 15 min each. The substrates were then dried in an oven at 70 °C. ITO substrates were exposed to UV/O_3 for 30 min in order to remove any remaining organic impurities. For the CNT anodes, bare glass substrates (Techno Print Co., Ltd.) were purchased and cleaned by the same method as the ITO substrates. Prior to CNT transfer, the substrates were exposed to UV/O_3 for 30 min. CNT was transferred using a pair of tweezers and a drop of ethanol was used to ensure firm adhesion of the CNTs. 30% water diluted HNO_3(aq) was applied for certain CNT films for doping effect. For the flexible devices, Toyobo ltd. polyethylene terephthalate (A4300-38 μm) were used. The films were cleaned by ethanol and clean gauze before CNT transfer. A drop of ethanol was used to ensure firm adhesion of the CNTs. Then the substrates were transferred to a nitrogen filled glove box for further fabrication. For the both-CNT-electrode devices, 2 mg mL^{-1} of P3HT in CB was applied and spin-coated at 4500 rpm for 45 s.

Perovskite solar cell fabrication. PEDOT:PSS was produced by adding 0.5 wt% ofpolyoxyethylene(6) tridecyl ether (Sigma Aldrich Chemical Co., Inc.) in poly-(3,4-ethylenedioxythiophene)-polystyrenesulfonic acid (PEDOT:PSS) dispersion in water (Clevios P VP, Heraeus Precious Metals GmbH & Co.). IPA-PEDOT:PSS was produced by diluting PEDOT:PSS in 2-isopropanol at 3:1(v/v) ratio. Modified PEDOT:PSS was spin coated at the same condition as the normal PEDOT:PSS which is 4500 rpm for 45 s. The $MAPbI_3$ perovskite layers were fabricated via Lewis base adduct method. A 1:1:1 molar ratio mixture of PbI_2 (TCI), MAI (TCI), and dimethyl sulfoxide (DMSO) (TCI) was dissolved in dimethylformamide (DMF) at 50 wt% without heating. The fully dissolved solution was spin coated onto the PEDOT:PSS

layer at 3500 rpm for 20 s, with a dropping of 0.3 mL diethyl ether 8s after starting the spin-coating process. The transparent green film, so-called CH_3NH_3I•PbI_2•DMSO adduct film, changed to a dark brown color by heating at 65 °C for 1 min and 100 °C for 4 min. For the reference device, thermal evaporation of C_{60}, BCP, LiF, and Al was followed to give 35 nm, 10 nm, 1nm, and 100 nm, respectively.

For the devices in which CNT is the cathode, CNT films were mechanically transferred to the top of the perovskite layer. A $PC_{61}BM$ solution, which was prepared by mixing 20 mg of $PC_{61}BM$ in 1 mL of CB, was applied directly on the laminated CNT film. Au was thermally deposited only at the edges to assist CNT contact.

Characterisations. *J–V* characteristics were measured by software-controlled source meter (Keithley 2400) in dark conditions and 1 sun AM 1.5G simulated sunlight irradiation (100 mW cm^{-2}) using a solar simulator (EMS-35AAA, Ushio Spax Inc.) with Ushio Xe short ark lamp 500, which was calibrated using a silicon diode (BS-520BK, Bunkokeiki). SEM measurement was carried out on S-4800 (Hitachi). Fermi levels were measured by Riken Keiki PYS-A AC-2 in air. Both homemade systems based on Seki Technotron STR-250 (excitation wavelength 532 nm) and inVia Raman microscope (Renishaw) were used for the Raman measurement. Shimadzu UV-3150 was used for the UV-vis-NIR measurement. IPCE system consisted of a MLS-1510 monochromator to scan the UV-vis spectrum. A source measurement unit was used to record the current at each specific wavelength. TEM and STEM images of CNT electrodes were obtained using a JEOL JEM-2100F electron microscope equipped with double JEOL Delta spherical aberration correctors at a reduced electron accelerating voltage of 60 kV to minimize irradiation-induced damage. EELS measurement was carried out using a Gatan Quantum electron spectrometer attached to the microscope. Elemental distributions of carbon and sulfur were

determined by the intensities of their K and L edges, respectively, at each measured point in the scanned areas for STEM-EELS chemical mapping.

RESULTS AND DISCUSSION

Simplified PSC architecture. Inverted-type planar-heterojunction PSCs have the advantages of low hysteresis and room-temperature processability over normal-type PSCs, which are crucial for commercial fabrication.[30,31] However, high-performance inverted PSCs still typically have vacuum-deposited layers, such as C_{60}, bathocuproine (BCP), or LiF. From the perspective of commercialization, such vacuum processes incur exorbitant setup and running costs. These can be avoided by using a solution-processed single layer of $PC_{61}BM$, which greatly simplifies the configuration at the expense of PCE (Figure 1a). According to our experimental results, the inverted-type PSCs with the vacuum-deposited electron-transporting layers (ETLs) had PCE of 17.2% (Figure 1b; Figure S1), while the PSCs with a single solution-processed $PC_{61}BM$ layer had PCE of 12.8% (Figure 1c; Figure S1). Despite this drop of 4.4%, the latter process had substantially lower fabrication costs, thus making it more industrially viable. The structure can be improved even further by replacing ITO and aluminum electrodes with carbon electrodes. ITO is unstable in acidic PEDOT:PSS[32] and undergoes a sputtering process at temperatures above 300 °C, which increases fabrication costs and limits the scope of application.[33] The top metal electrode is also vacuum-deposited and prone to oxidization in air. Therefore, we propose the use of CNTs as both the anode and the cathode to replace the conventional electrodes (Figure 1a).[34] Using the two CNT electrodes and entirely solution-processable layers between the electrodes will promote innovation in processing technology. A continuous R2P production could lead to

dramatic cost reductions and high throughput, potentially revolutionizing the manufacture of thin-film solar cells.

CNT as an anode and a cathode in PSCs. To achieve the both-CNT-electrode architecture, demonstration of CNTs separately as the anode and the cathode is necessary (Figure 1d). For CNT anode-based PSCs, we used transparent CNT films (*ca*. 90% transmittance at 550 nm wavelength) and doped the film using HNO_3 to enhance its conductivity (Figure S2). We used a similar approach in our previous study.[10] However, in the present study, we fabricated $MAPbI_3$ using the adduct method, which gave higher efficiency[35] and produced a PCE of 9.8% (Figure 1e and S1). Furthermore, a CNT film was used as the cathode to replace the metal electrode. Because $MAPbI_3$ absorbs most of the solar spectrum, dark and dense CNT films were used for their high conductivity (Table S1 and Figure S2). When a CNT film is laminated as the top electrode, interfacial contact is crucial. In general, a few droplets of chlorobenzene (CB) on CNT films improve the contact between the CNT film and $MAPbI_3$.[36] In this study, we used a solution of $PC_{61}BM$ in CB. Applying $PC_{61}BM$ solution directly onto the CNT top electrode improved both the interfacial contact and the electron-transporting ability of the devices. In fact, the application of $PC_{61}BM$ solution after CNT lamination produced better performance compared with the application of $PC_{61}BM$ solution, both before and after CNT lamination (Figure S3) and a PCE of 10.5% was recorded. Interestingly, PSCs with a CNT film as the cathode performed better than those with a CNT film as the anode (Figure 1f and S1). The difference arose from the fill factor (FF), which chiefly reflects the difference in conductivity between the CNT films. Moreover, application of the $PC_{61}BM$ solution to CNT film enhanced conductivity. We conjecture that this was due to a doping effect, which is addressed in the Discussion section.

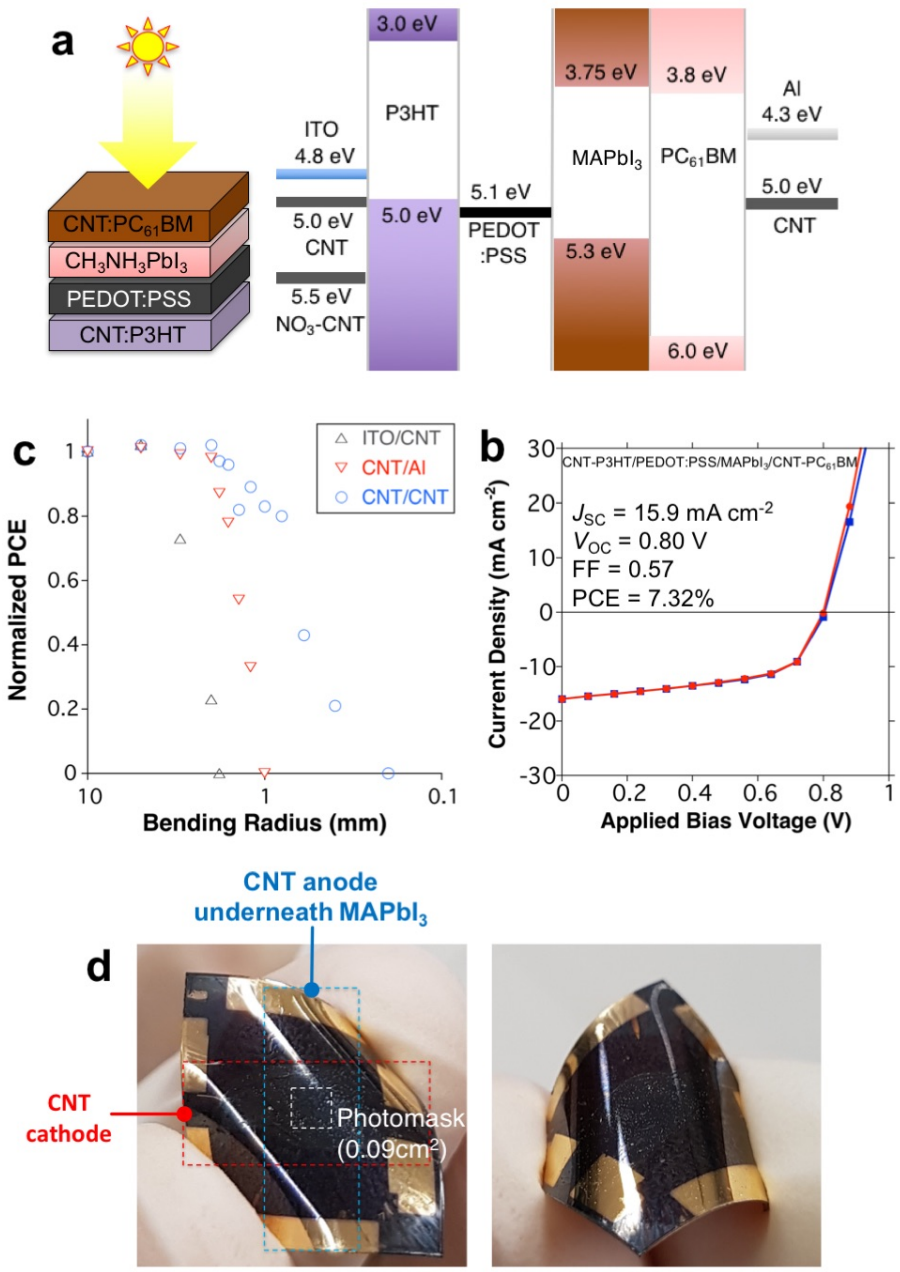

Figure 2. (**a**) Schematic illustrations of a both-CNT-electrode PSC and its energy level diagram. (**b**) Forward (red) and reverse (blue) bias *J*–*V* curves with photovoltaic parameters. (**c**) Bending radius test of the CNT cathode devices (ITO/CNT), the CNT anode devices (CNT/Al), and the both-CNT-electrode devices. (**d**) Photos of the both-CNT-electrode PSC.

Using both CNT electrodes in a PSC. Having successfully demonstrated the application of CNT films as both the anode and the cathode in PSCs, we fabricated both-CNT-electrode PSCs. The devices were fabricated with a configuration of HNO_3-doped CNT/PEDOT:PSS/$MAPbI_3$/$PC_{61}BM$/CNT. However, they appeared to be short-circuited (Figure S4). Because the current density and voltage (*J–V*) curve showed an ohmic contact, there was possibly an energy misalignment. Previously, both-carbon-electrode systems have been demonstrated by means of energy band modification,[37–42] and so we used different materials to control the energy bands of the both-CNT-electrode system. We found that the combination of P3HT-soaked CNT and $PC_{61}BM$-soaked CNT without use of nitric acid dopant was favorable (Figure 2a, Figure S5). A dense CNT film was soaked in a low-concentration solution of P3HT (2 mg mL^{-1}) and a solar light was shone from the $PC_{61}BM$-treated transparent CNT side to maximize the solar absorption (Figure S6). This also avoided the light passing through the substrate, thus avoiding possible light loss in flexible devices, as the lower transmittance of flexible plastic substrates usually leads to lower performance (Figure S7).[9] A PCE of 7.32% was produced by the both-CNT-electrode PSCs (Figure 2b, Figure S8). Compared with the single-CNT-electrode devices, the both-CNT-electrode devices had a relatively low FF. This was attributed to the lower conductivity of the CNT films compared with ITO or metal (Table S1). Also, the relatively lower J_{sc} was due to the lower transmittance of the $PC_{61}BM$-soaked CNT electrode compared with ITO, and possibly to unoptimized energy levels. This suggests that improvement of CNT quality and structural optimization can increase the PCE further. Polyethylene terephthalate (PET) substrates were used to produce flexible devices (Table S1). The flexible both-CNT-electrode PSCs gave PCE comparable to that of glass substrate-based devices (*ca.* 7.04%). This is because there was no light loss due to the plastic substrate, and the

polar perovskite solvent did not react with the plastic substrate, unlike in organic solar cells, where a reactive nonpolar solvent is used for the active materials. According to the bending radius test in Figure 2c and d, the both-CNT-electrode PSCs had better flexibility than did the PSCs with either ITO/CNT or CNT/Al electrodes. This might be explained by the flexible ITO starting to crack when bent more than 60°[43] and also by metal electrodes peeling off due to poor adhesion.[9]

Investigation of CNT electrodes and the doping effect. Next, the CNT electrodes were analyzed by transmission electron microscopy (TEM). From the images of the $PC_{61}BM$-soaked CNT film (Figure 3a, Figure S9), we can see that $PC_{61}BM$ molecules thoroughly penetrated into the CNT network, due to their small size and strong π–π interactions with the CNTs. From the images of P3HT-soaked CNT films (Figure 3b, Figure S10), we can see P3HT wrapping around CNTs, again through π–π interactions. Electron energy loss spectroscopy (EELS) chemical mapping combined with scanning TEM (STEM) confirmed that the P3HT polymer was indeed wrapped around the CNTs.[44,45] The doping effect in these CNT electrodes was investigated by four-probe measurement, Raman spectroscopy, near-infrared spectroscopy, and photoelectron yield spectroscopy (PYS). According to the Raman spectra, the addition of $PC_{61}BM$ to a pristine CNT film shifts both the G band (G^- band) and the 2D band to lower wavenumber (Figure 3c and d). This indicates an *n*-type doping effect of $PC_{61}BM$ on CNTs.[46,47] This is a surprising discovery since fullerene is thought to accept electrons from CNTs.[37,38] However, those previous reports used semiconducting CNTs, in contrast to the mixture of metallic and semiconducting CNTs used in this work, and also did not comprehensively analyze CNT-$PC_{61}BM$. We plan to study this issue further in a future project. Regardless of the type of doping, the doping itself was confirmed by both four-probe measurement (Table S1) and near-infrared spectroscopy. The sheet resistance

(R_{Sheet}) of the CNT films decreased by approximately 200 Ω sq.$^{-1}$ and 20 Ω sq.$^{-1}$ for T90%-CNT film and T50%-CNT, respectively, upon $PC_{61}BM$ addition. On the other hand, P3HT did not produce a significant change when added to CNT films. According to near-infrared spectroscopy, $PC_{61}BM$-treated CNT showed slight decreases in van Hove transitions (Figure S11).[29] PYS measurement was used to find the Fermi levels of the nanocomposites, but the values of -6.4 eV and -4.6 eV for CNT-$PC_{61}BM$ and CNT-P3HT seemed to correspond to the highest occupied molecular orbitals of $PC_{61}BM$ and P3HT, respectively (Figure S12).

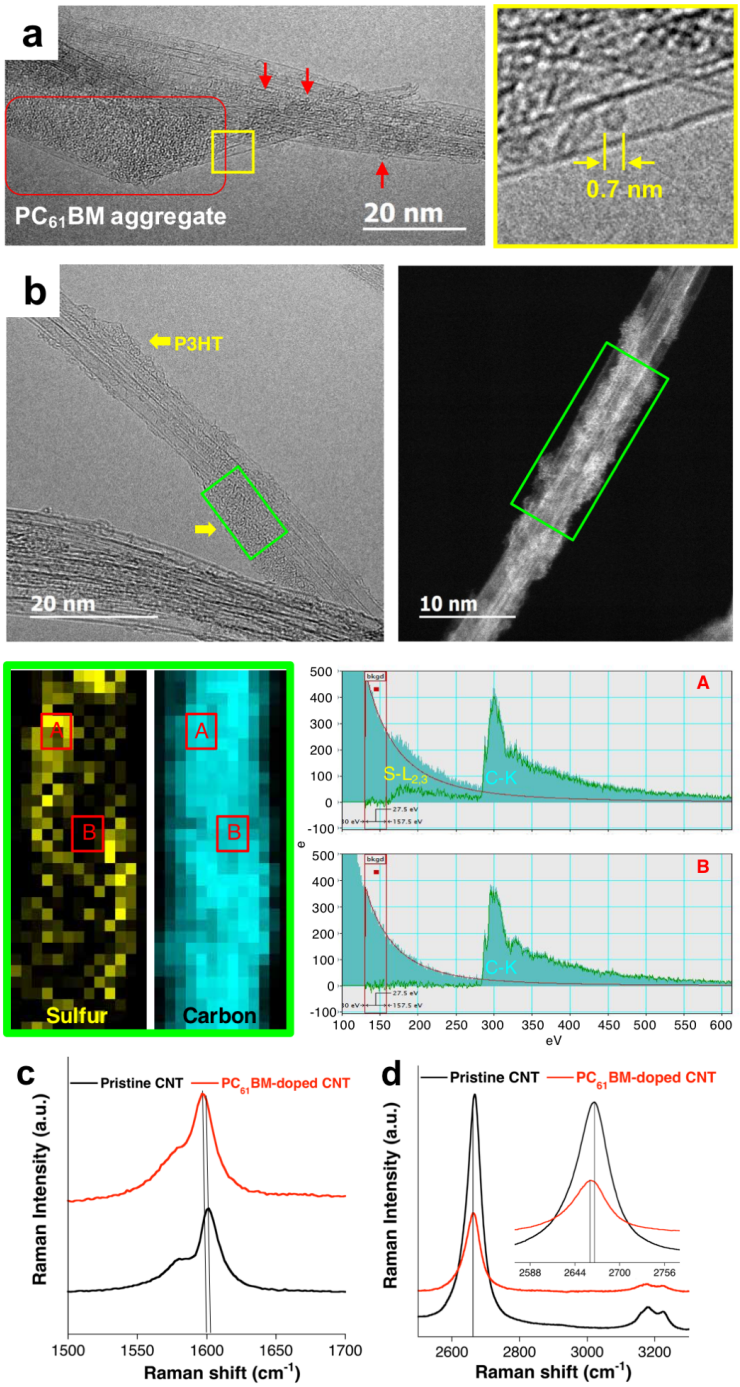

Figure 3. TEM images of (**a**) a CNT-$PC_{61}BM$ film and (**b**) a CNT-P3HT film. EELS chemical maps of sulfur and carbon (b, bottom left) correspond to the area indicated by the green rectangle in the STEM image (b, top right). Raman spectroscopy of CNT-$PC_{61}BM$ and pristine CNT films for (**c**) G band and (**d**) 2D band.

Process innovation by both-CNT-electrode PSCs. When considering the industrial viability of solar cells and their fabrication processes, PCE is not a sole factor to consider. The cost of fabrication, which encompasses material and setup costs and Takt time (processing time) are more important. PSCs are often presented as a low-cost solution-processable technology, but the reality is that conventional PSCs are prepared by complex and cumbersome processes, such as vacuum deposition, with slow and damage-inducing R2R processing.[34] It is vital that devices are highly compatible with high-speed printing at all levels, on a simple processing line.[26] Figure 4a shows a schematic for the conventional process, which is long and complicated and involves roll-back for vacuum chamber processing. This increases the processing time and causes damage due to bending, static electricity, and physical contact with the substrates of other layers.[22] Figure 4b shows the processing schematic of the both-CNT-electrode PSCs. Because of these new devices being either imprinted or slot dye coated entirely, the process is continuous, fast, and damage-free. As the process does not involve rollback during processing, using a glass substrate does not incur increased fabrication costs. Thus, both R2P and sheet-to-product processes are applicable. The speed of processing is directly related to the production cost. One slow step in a process slows down all of the inline processing. In R2P processing (Figure 4b), production of CNTs is the slowest process, but this process is done on a separate line. In the conventional processing (Figure 4a), non-continuous R2R processing, high-temperature annealing, and sputtering drastically increase the Takt time. This is exacerbated if non-flexible substrates are used, because S2S processing is much slower than R2R processing when vacuum chambers are involved.

Cost analysis. Cost of fabrication based on the actual prices and amounts of materials used for fabrication were analyzed (Table S2). It was important to input real data with minimal

assumptions, because the accuracy of the small-scale analysis is critical for an accurate extrapolation to mass production scale. In our estimation, we assumed that all devices are interconnected in series to form a module, as monolithic interconnection is a generally used concept in thin film module technology.[48] Therefore, the interconnecting area that does not contribute to the electricity generation is disregarded. Additionally, material switch gears, which take up a significant portion of electricity consumption, were omitted to avoid the cost estimation being overly favorable to the new process.[11] According to our analysis, both-CNT-electrode PSCs required a material cost that was 57.6% of that required by conventional devices. When scaled up by a factor of 10,000, the difference was even more significant and the material cost was only 32.9% of that required by conventional devices. If the setup costs, maintenance costs, and Takt time had also been taken into consideration, then difference would have been much greater. Moreover, with further optimization of the materials and design of the device, we are confident that the efficiency will increase, resulting in the performance outweighing fabrication costs by a considerable margin.

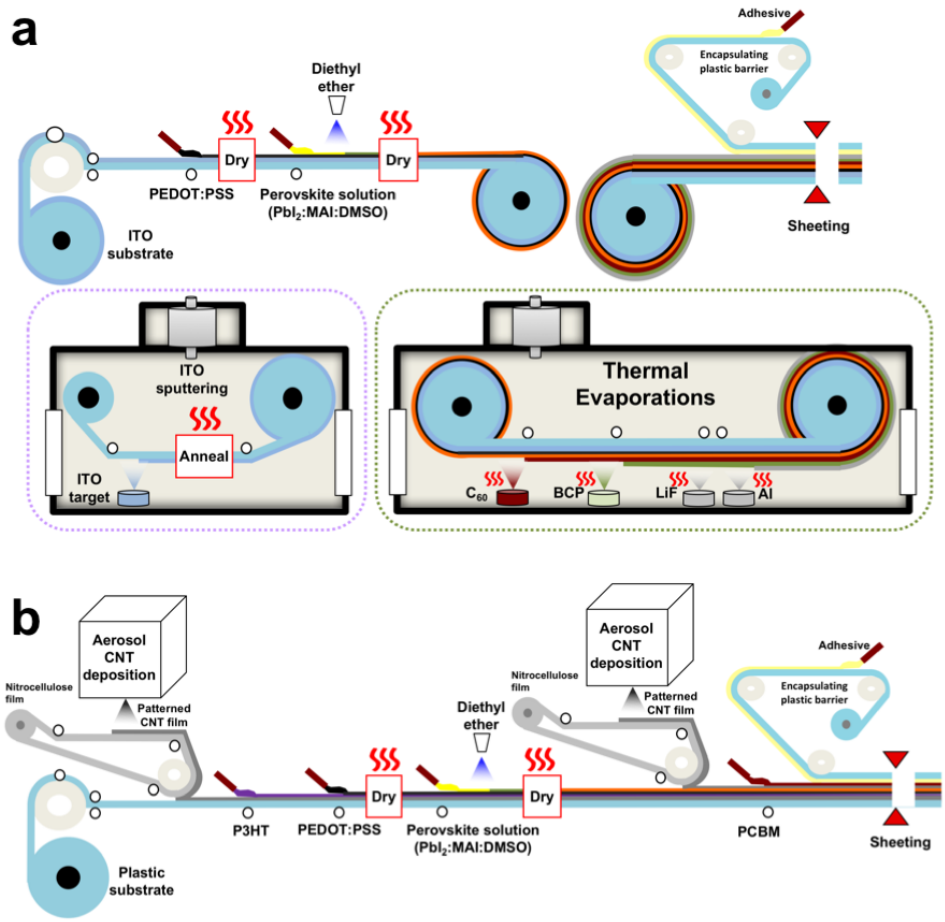

Figure 4. Process schematics of (**a**) conventional inverted-type PSCs and (**b**) both-CNT-electrode PSCs.

CONCLUSIONS

To compete with silicon solar cells, which are a mature technology, a dramatic cost reduction is necessary. However, the conventional PSC structure cannot exploit the full potential of solution processability. This study has demonstrated fabrication of both-CNT-electrode PSCs, with CNT films functioning as the anode and cathode in a single device. In addition, what is

currently postulated to be an *n*-type doping effect of $PC_{61}BM$ on CNTs has been discovered. The both-CNT-electrode PSCs have the advantages of low consumption of the raw materials and energy by enabling vacuum-free, high throughput, and continuous R2P processing. We believe that improvements in CNT quality and structural optimization can improve the PCE of these PSCs. Moreover, this work represents a step forward toward the use of all-carbon solar devices.

AUTHOR INFORMATION

Corresponding Author

Correspondence to: esko.kauppinen@aalto.fi, +358 40-509-8064 (E.K), maruyama@t.u-photon.ac.jp, +81 3-5841-6421 (S.M.), matsuo@photon.t.u-tokyo.ac.jp, +81 3-5841-0978 (Y.M.)

Notes

The authors declare no competing financial interests. † These authors contributed equally (I.J. and S.S.).

Supporting Information

Supporting information contains incident photon-to-electron conversion efficiency measurements, four-probe sheet resistance measurements, UV-vis transmittance measurements, *J–V* curves of unsuccessful both-CNT-electrode PSC, SEM images, TEM images, near-infrared spectra, PYS measurements, cost analysis table, and statistical analysis.

ACKNOWLEDGMENTS

I.J. thanks the Research and Education Consortium for Innovation of Advanced Integrated Science by Japan Science and Technology (JST). This work was supported by Japan Society for the Promotion of Science (JSPS) KAKENHI Grant Numbers JP25107002, JP15H05760, JP16H04187, JP17K19116, JP17H06609 and IRENA Project by JST-EC DG RTD, Strategic International Collaborative Research Program, SICORP. Part of this work is based on results obtained from a project commissioned by the New Energy and Industrial Technology Development Organization (NEDO). This work was partly supported by the MOPPI project of the Aalto University AEF research program.

REFERENCES

(1) Green, M. A.; Ho-Baillie, A.; Snaith, H. J. The emergence of perovskite solar cells. *Nat. Photonics* **2014**, *8*, 506-514

(2) McGehee, M. D. Perovskite solar cells: Continuing to soar. *Nat. Mater.* **2014**, *13*, 845-6.

(3) Kim, H.-S.; Lee, C.-R.; Im, J.-H.; Lee, K.-B.; Moehl, T.; Marchioro, A.; Moon, S.-J.; Humphry-Baker, R.; Yum, J.-H.; Moser, J. E.; *et al*. Lead iodide perovskite sensitized all-solid-state submicron thin film mesoscopic solar cell with efficiency exceeding 9%. *Sci. Rep.* **2012**, *2*, 591.

(4) Kojima, A.; Teshima, K.; Shirai, Y.; Miyasaka, T. Organometal halide perovskites as visible-light sensitizers for photovoltaic cells. *J. Am. Chem. Soc.* **2009**, *131*, 6050-6051.

(5) Li, X.; Bi, D.; Yi, C.; Decoppet, J.-D.; Luo, J.; Zakeeruddin, S. M.; Hagfeldt, A.; Grätzel, M. A vacuum flash-assisted solution process for high-efficiency large-area perovskite solar cells. *Science* **2016**, *353*, 58-62.

(6) Seo, J.; Noh, J. H.; Seok, S. Il. Rational strategies for efficient perovskite solar cells. *Acc. Chem. Res.* **2016**, *49*, 562-572.

(7) Bi, D.; Tress, W.; Dar, M. I.; Gao, P.; Luo, J.; Renevier, C.; Schenk, K.; Abate, A.; Giordano, F.; Correa Baena, J.-P.; *et al*. Efficient luminescent solar cells based on tailored mixed-cation perovskites. *Sci. Adv.* **2016**, *2*, e1501170.

(8) Yang, W. S.; Noh, J. H.; Jeon, N. J.; Kim, Y. C.; Ryu, S.; Seo, J.; Seok, S. Il. High-performance photovoltaic perovskite layers fabricated through intramolecular exchange. *Science* **2015**, *348*, 1234-1237.

(9) Yoon, J.; Sung, H.; Lee, G.; Cho, W.; Ahn, N.; Jung, H. S.; Choi, M. Superflexible, high-efficiency perovskite solar cells utilizing graphene electrodes: towards future foldable power sources. *Energy Environ. Sci.* **2017**, *10*, 337-345.

(10) Jeon, I.; Chiba, T.; Delacou, C.; Guo, Y.; Kaskela, A.; Reynaud, O.; Kauppinen, E. I.; Maruyama, S.; Matsuo, Y. Single-walled carbon nanotube film as electrode in indium-free planar heterojunction perovskite solar cells: investigation of electron-blocking layers and dopants. *Nano Lett.* **2015**, *15*, 6665-6671.

(11) Azzopardi, B.; Emmott, C. J. M.; Urbina, A.; Krebs, F. C.; Mutale, J.; Nelson, J. Economic assessment of solar electricity production from organic-based photovoltaic modules in a domestic environment. *Energy Environ. Sci.* **2011**, *4*, 3741-3753.

(12) Azzopardi, B. Future development promise for plastic-based solar electricity. *Progress in Photovoltaics: Research and Applications*. **2016**, *2*, 261-268.

(13) Sung, H.; Ahn, N.; Jang, M. S.; Lee, J.; Yoon, H.; Park, N.; Choi, M. Transparent conductive oxide-free graphene-based perovskite solar cells with over 17% efficiency. *Adv. Energy Mater*. **2016**, *6*, 1501873.

(14) Espinosa, N.; Hösel, M.; Angmo, D.; Krebs, F. C. Solar cells with one-day energy payback for the factories of the future. *Energy Environ. Sci.* **2012**, *5*, 5117-5132.

(15) Søndergaard, R.; Hösel, M.; Angmo, D.; Larsen-Olsen, T. T.; Krebs, F. C. Roll-to-roll fabrication of polymer solar cells. *Materials Today*. **2012**, *15*, 36-49.

(16) Schmidt, T. M.; Larsen-Olsen, T. T.; Carlé, J. E.; Angmo, D.; Krebs, F. C. Upscaling of perovskite solar cells: fully ambient roll processing of flexible perovskite solar cells with printed back electrodes. *Adv. Energy Mater.* **2015**, *5*, 1500569.

(17) Machui, F.; Hösel, M.; Li, N.; Spyropoulos, G. D.; Ameri, T.; Søndergaard, R. R.; Jørgensen, M.; Scheel, A.; Gaiser, D.; Kreul, K.; *et al*. Cost analysis of roll-to-roll fabricated ITO free single and tandem organic solar modules based on data from manufacture. *Energy Environ. Sci.* **2014**, *7*, 2792-2802.

(18) Hösel, M.; Angmo, D.; Søndergaard, R. R.; dos Reis Benatto, G. a.; Carlé, J. E.; Jørgensen, M.; Krebs, F. C. High-volume processed, ITO-free superstrates and substrates for roll-to-roll development of organic electronics. *Adv. Sci.* **2014**, *1*, 1400002.

(19) Søndergaard, R. R.; Hösel, M.; Krebs, F. C. Roll-to-roll fabrication of large area functional organic materials. *J. Polym. Sci. Part B Polym. Phys.* **2013**, *51*, 16-34.

(20) Hösel, M.; Søndergaard, R. R.; Jørgensen, M.; Krebs, F. C. Comparison of UV curing, hotmelt, and pressure sensitive adhesive as roll-to-roll encapsulation methods for polymer solar cells. *Adv. Eng. Mater.* **2013**, *15*, 1068-1075.

(21) Krebs, F. C. Fabrication and processing of polymer solar cells: A review of printing and coating techniques. *Sol. Energy Mater. Sol. Cells* **2009**, *93*, 394-412.

(22) Robinson, K.; Durkin, W. Electrostatic issues in roll-to-roll manufacturing operations. *IEEE Trans. Ind. Appl.* **2010**, *46*, 2172-2178.

(23) Hwang, S. Y.; Hong, S. H.; Jung, H. Y.; Lee, H. Fabrication of roll imprint stamp for continuous UV roll imprinting process. *Microelectron. Eng.* **2009**, *86*, 642-645.

(24) Ahn, S. H.; Guo, L. J. Large-area roll-to-roll and roll-to-plate nanoimprint lithography: a step toward high-throughput application of continuous nanoimprinting. *ACS Nano* **2009**, *3*, 2304-2310.

(25) Krebs, F. C. All solution roll-to-roll processed polymer solar cells free from indium-tin-oxide and vacuum coating steps. *Org. Electron.* **2009**, *10*, 761-768.

(26) Larsen-Olsen, T. T.; Søndergaard, R. R.; Norrman, K.; Jørgensen, M.; Krebs, F. C. All printed transparent electrodes through an electrical switching mechanism: a convincing alternative to indium-tin-oxide, silver and vacuum. *Energy Environ. Sci.* **2012**, *5*, 9467-9471.

(27) Jeon, I.; Delacou, C.; Kaskela, A.; Kauppinen, E. I.; Maruyama, S.; Matsuo, Y. Metal-electrode-free window-like organic solar cells with p-doped carbon nanotube thin-film electrodes. *Sci. Rep.* **2016**, *6*, 31348.

(28) Li, Z.; Kulkarni, S. A.; Boix, P. P.; Shi, E.; Cao, A.; Fu, K.; Batabyal, S. K.; Zhang, J.; Xiong, Q.; Wong, L. H.; *et al*. Laminated carbon nanotube networks for metal electrode-free efficient perovskite solar cells. *ACS Nano* **2014**, *8*, 6797-6804.

(29) Jeon, I.; Cui, K.; Chiba, T.; Anisimov, A.; Nasibulin, A. G.; Kauppinen, E. I.; Maruyama, S.; Matsuo, Y. Direct and dry deposited single-walled carbon nanotube films doped with MoOx

as electron-blocking transparent electrodes for flexible organic solar cells. *J. Am. Chem. Soc.* **2015**, *137*, 7982-7985.

(30) Docampo, P.; Ball, J. M.; Darwich, M.; Eperon, G. E.; Snaith, H. J. Efficient organometal trihalide perovskite planar-heterojunction solar cells on flexible polymer substrates. *Nat. Commun.* **2013**, *4*, 2761.

(31) Wu, C.-G.; Chiang, C.-H.; Tseng, Z.-L.; Nazeeruddin, M. K.; Hagfeldt, A.; Grätzel, M. High efficiency stable inverted perovskite solar cells without current hysteresis. *Energy Environ. Sci.* **2015**, *8*, 2725-2733.

(32) Guo, C. X.; Guai, G. H.; Li, C. M. Graphene based materials: enhancing solar energy harvesting. *Adv. Energy Mater.* **2011**, *1*, 448-452.

(33) Salvatierra, R. V.; Cava, C. E.; Roman, L. S.; Zarbin, A. J. G. ITO free and flexible organic photovoltaic device based on high transparent and conductive polyaniline/carbon nanotube thin films. *Adv. Funct. Mater.* **2013**, *23*, 1490-1499.

(34) Krebs, F. C.; Tromholt, T.; Jørgensen, M. Upscaling of polymer solar cell fabrication using full roll-to-roll processing. *Nanoscale* **2010**, *2*, 873-886.

(35) Ahn, N.; Son, D.-Y.; Jang, I.-H.; Kang, S. M.; Choi, M.; Park, N. Highly reproducible perovskite solar cells with average efficiency of 18.3% and best efficiency of 19.7% fabricated via Lewis base adduct of lead (II) iodide. *J. Am. Chem. Soc.* **2015**, *137*, 8696-8699.

(36) Lee, Y.; Tu, K.-H.; Yu, C.; Li, S.; Hwang, J.-Y.; Lin, C.; Chen, K.-H.; Chen, L.-C.; Chen, H.-L.; Chen, C.-W. Top laminated graphene electrode in a semitransparent polymer solar cell by simultaneous thermal annealing/releasing method. *ACS Nano* **2011**, *5*, 6564-6570.

(37) Cells, A. S.; Ramuz, M. P.; Vosgueritchian, M.; Wei, P.; Wang, C.; Gao, Y.; Wu, Y.; Chen, Y.; Bao, Z. Evaluation of solution-processable carbon-based electrodes for all-carbon solar cells. *ACS Nano* **2012**, *6*, 10384-10395.

(38) Tung, V. C.; Huang, J.-H. J.; Kim, J.; Smith, A. J.; Chu, C.-W.; Huang, J.-H. J. Towards solution processed all-carbon solar cells: a perspective. *Energy Environ. Sci.* **2012**, *5*, 7810-7818.

(39) Song, Y.; Chang, S.; Gradecak, S.; Kong, J. Visibly-transparent organic solar cells on flexible substrates with all-graphene electrodes. *Adv. Energy Mater.* **2016**, *6*, 1600847.

(40) Liu, Z.; You, P.; Liu, S.; Yan, F. Neutral-color semitransparent organic solar cells with all-graphene electrodes. *ACS Nano* **2015**, *9*, 12026-12034.

(41) Kyaw, A. K. K.; Tantang, H.; Wu, T.; Ke, L.; Wei, J.; Demir, H. V.; Zhang, Q.; Sun, X. W. Dye-sensitized solar cell with a pair of carbon-based electrodes. *J. Phys. D. Appl. Phys.* **2012**, *45*, 165103.

(42) Cai, X.; Hou, S.; Wu, H.; Lv, Z.; Fu, Y.; Wang, D.; Zhang, C.; Kafafy, H.; Chu, Z.; Zou, D. All-carbon electrode-based fiber-shaped dye-sensitized solar cells. *Phys. Chem. Chem. Phys.* **2012**, *14*, 125-130.

(43) You, J.; Hong, Z.; Yang, Y. (Michael); Chen, Q.; Cai, M.; Song, T.-B.; Chen, C.-C.; Lu, S.; Liu, Y.; Zhou, H.; *et al*. Low-temperature solution-processed perovskite solar cells with high efficiency and flexibility. *ACS Nano* **2014**, *8*, 1674-1680.

(44) Lee, H. W.; Yoon, Y.; Park, S.; Oh, J. H.; Hong, S.; Liyanage, L. S.; Wang, H.; Morishita, S.; Patil, N.; Park, Y. J.; *et al*. Selective dispersion of high purity semiconducting single-walled carbon nanotubes with regioregular poly(3-alkylthiophene)s. *Nat. Commun.* **2011**, *2*, 541.

(45) Stranks, S. D.; Yong, C.-K.; Alexander-Webber, J. A.; Weisspfennig, C.; Johnston, M. B.; Herz, L. M.; Nicholas, R. J. Nanoengineering coaxial carbon nanotube–dual-polymer heterostructures. *ACS Nano* **2012**, *6*, 6058-6066.

(46) Bissett, M. A.; Konabe, S.; Okada, S.; Tsuji, M.; Ago, H. Enhanced chemical reactivity of graphene induced by mechanical strain. *ACS Nano* **2013**, *7*, 10335-10343.

(47) Koehler, F. M.; Luechinger, N. A.; Ziegler, D.; Athanassiou, E. K.; Grass, R. N.; Rossi, A.; Hierold, C.; Stemmer, A.; Stark, W. J. Permanent pattern resolved adjustment of the surface potential of graphene like carbon through chemical functionalization. *Angew. Chem. Int. Ed.* **2009**, *48*, 224-227.

(48) Barr, M. C.; Rowehl, J. A.; Lunt, R. R.; Xu, J.; Wang, A.; Boyce, C. M.; Im, S. G.; Bulović, V.; Gleason, K. K. Direct monolithic integration of organic photovoltaic circuits on unmodified paper. *Adv. Mater.* **2011**, *23*, 3500.

TOC Graphic

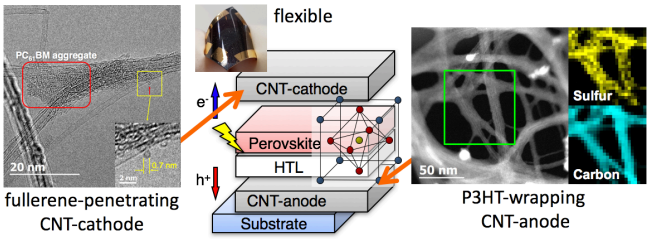
flexible
CNT-cathode
e⁻
Perovskite
HTL
h⁺
CNT-anode
Substrate
20 nm
fullerene-penetrating
CNT-cathode
Sulfur
Carbon
50 nm
P3HT-wrapping
CNT-anode